A combined tactile and Raman probe for tissue characterization - Design considerations

A combined tactile and Raman probe for tissue characterization – Design considerations

Morgan Nyberg[1,2], Stefan Candefjord[1-4], Ville Jalkanen[2,5], Kerstin Ramser[1,2], and Olof A Lindahl[1,2,6]

[1]Department of Computer Science, Electrical and Space Engineering, Luleå University of Technology, 971 87 Luleå, Sweden

[2]Centre for Biomedical Engineering and Physics, Luleå University of Technology and Umeå University, Luleå and Umeå, Sweden

[3]Signals and Systems, Chalmers University of Technology, 412 96, Gothenburg, Sweden

[4]MedTech West, Sahlgrenska University Hospital, Blå Stråket 7, 413 45, Gothenburg, Sweden

[5]Department of Applied Physics and Electronics, Umeå University, 901 87 Umeå, Sweden

[6]Department of Radiation Sciences/Biomedical Engineering, Umeå University, 901 87 Umeå, Sweden

Abstract

Histopathology is the golden standard for cancer diagnosis and involves the characterization of tissue components. It is labor intensive and time consuming. We have earlier proposed a combined fibre-optic near-infrared Raman spectroscopy (NIR-RS) and tactile resonance method (TRM) probe for detecting positive surgical margins as a complement to interoperative histopathology. The aims of this study were to investigate the effects of attaching an RS probe inside a cylindrical TRM sensor, to investigate how laser-induced heat of the fibre-optic NIR-RS affected the temperature of the RS probe tip and an encasing TRM sensor. In addition, the possibility to perform fibre-optic NIR-RS in a well-lit environment was investigated.

A small amount of rubber latex was preferable for attaching the thin RS probe inside the TRM sensor. The temperature rise of the TRM sensor due to a fibre-optic NIR-RS at 270 mW during 20 s was less than 2 °C. Fibre-optic NIR-RS was feasible in a dimmed bright environment using a small light shield and automatic subtraction of a pre-recorded contaminant spectrum. The results are promising for a combined probe for tissue characterization.

List of abbreviations

Δf	Frequency shift
f_0	Non-contact resonance frequency
NIR	Near infrared
PCa	Prostate cancer
PSA	Prostate specific antigen

PSM	Positive surgical margin
PZT	Lead zirconium titanate
RP	Radical prostatectomy
RS	Raman spectroscopy
TRM	Tactile resonance method

1. Introduction

The golden standard of tissue characterization is microscopic histopathology. Complementary methods emerge as technology advances. Among several emerging methods, Raman spectroscopy (RS) and the tactile resonance method (TRM) show individually promising results for tissue characterization. RS has been shown to differentiate tissue types in terms of their molecular composition, and is also able to classify epithelial cancers and pre-cancers [1, 2]. TRM has been used to investigate lymph nodes, liver cirrhosis and skin hardness [3, 4, 5]. Both fibre-optic NIR-RS and TRM has shown promising results for prostate cancer detection and diagnosis [6, 7]. Jalkanen *et al.* suggested that TRM could be combined with other techniques to increase the diagnostic accuracy of prostatic diseases [8]. A combination of the TRM and RS technologies would be beneficial in many fields of tissue characterization. Both have certain drawbacks that might impair their clinical performance, but their combination may compensate for the drawbacks. RS can be performed relatively fast but does not give immediate results, and the measurement area is small when using fibre-optic RS. TRM senses tissue stiffness, but tissue structures with equal stiffness's might be of different compositions and necessary to discern. A recent study by Candefjord *et al.* [9], in which RS and TRM were compared by concurrent measurements of the same tissue sample, suggested that an integration of the two techniques would be beneficial for quick and accurate biological analysis. TRM could be used to immediate discern regions containing tumours and other stiffer tissues while RS could be used discriminately on stiffer tissue to determine the molecular content. Together, these techniques are promising e.g., for intraoperative examination of surgical margins as well as for histopathological analysis in general.

A combined tactile and RS probe, as suggested by us [9], consists of a tube shaped ceramic piezoelectric element as the TRM sensor, and a thin fibre-optic RS probe. A number of important basic factors are then necessary to consider when designing a combined probe. It is important to investigate how the individual measurement parameters could be affected by each other and the methods used while fabricating the combined instrument. For example, fibre-optic NIR-RS is a very precise technique, but to maintain a good signal-to-background ratio, a shorter measurement time has to be balanced against a higher laser output power. This is because the RS signal quality improves with higher laser power and longer integration time, while a high laser output power might cause tissue damage due to heating or photo-chemistry [10]. Moreover, a shorter measurement time is preferable for a handheld device.

Another obstacle is that the Raman scattering is a weak phenomenon. Only one out of 10^6 incident photons obtains a frequency shift [11]. This means that it is sensitive to surrounding light, and therefore fibre-optic RS is usually performed in dark environments. As a clinical instrument, the combined probe has to perform in bright environments such as an operation room. The effects of the surrounding light must therefore be suppressed in the design of the combined instrument.

The fibre-optic RS probe, suggested to be used in the combined instrument, is constructed with a filter and a lens attached to the probe tip [12]. These attachments will be heated by the transmitted laser [10]. The induced heat might be transmitted to the TRM sensor, which might be a cause of concern as the piezoelectric element is affected by temperature variations [13]. Moreover, the combined clinical probe would be used in environments where the temperature cannot be exactly controlled. These variations may be caused by: fluctuations of the ambient temperature, measurement samples of different temperatures, or heat induced by the exciting laser of the fibre-optic RS [10, 14].

It is suggested that the TRM sensor will be cemented inside the cylindrical RS probe. However, this can affect the TRM parameter, the resonance frequency, which changes when a mass is attached to the resonance sensor system [13].

The aim of this study was to take the concept of the combined probe further by identifying the specific drawbacks in the above mentioned situations and to overcome them by identifying feasible solutions.

2. Material and methods

2.1. Silicone and porcine samples

When investigating the temperature dependence of a TRM sensor, a silicone sample was used as a model system. The silicone (WackerSilGel 612, Wacker-Chemie GmbH, Munich, Germany) was prepared in a Petri dish (∅87 mm, height 13 mm) in a 4:3.5 ratio, which yields a stiffness of 192 mm×10^{-1} (DIN ISO 2137, hollow cone 150 g) [15]. The surface was coated with a thin layer of aluminium powder (Buehler, Lake Bluff, IL 60044, USA) to prevent the sensor tip from adhering to the surface [8].

When the impact of ambient light was investigated, porcine tissue, muscle + fat, was chosen as biological sample. Cut pork loin fillet was purchased at the local store and kept frozen at -23°C. Single cuts were thawed at 6 °C the day of measurement and each muscle tissue sample was cut 12 mm thick with approximately 40 mm and 50 mm sides.

2.2. Cylindrical tactile resonance sensor element

The TRM sensor intended for the combined probe is a lead zirconium titanate (PZT) ceramic: 15 mm long, 5 mm outer diameter, 2.8 mm inner diameter (Morgan Electro Ceramics, Bedford, OH, USA). It consists of a tube shaped PZT element coated with a thin, conductive film. The conductive film is cut in two separate regions, one for driving the vibration of the PZT element and another for picking up the vibration frequency (figure 1).

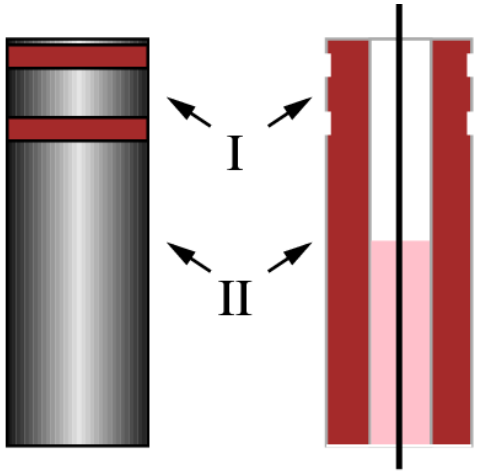

Figure 1. (Left) Side view of a tube-shaped piezoelectric element (red colour) coated with thin conductive film (gray). (Right) Cross sectional view with thin a steel pipe (black line) cemented in the middle by filling the cavity half-full with rubber latex (pink). Pick-up electrode (I), and drive electrode (II).

2.3. Fibre-optic RS probe

A fibre-optic probe (Machida Endoscope Co, Tokyo, Japan) was connected to a Kaiser Optical System Raman spectroscope (RXN1/0002134, USA). The optical fibres of the probe consist of pure fused silica [12]. The 785 nm laser light is delivered by one central fibre, and the scattered laser light is collected by

eight surrounding fibres [12]. The RS probe ends with a 10 cm-long steel pipe, in which the optical fibres are embedded. Two probes were used, one with outer diameter of the steel pipe 0.8 mm and one 1.2 mm. Both RS probes have a filter and a lens attached at the tip [12]. The 0.8-mm fibre-optic probe was used for measurements performed in bright environments. Laser powers between 100 and 270 mW, and integration times between 5 and 20 s were used. The laser powers refer to the power at the source. The output power was approx. 50% of the source power for both probes.

2.4. RS data pre-processing

The Raman spectra were analysed in the finger-print region of 400 cm^{-1} to 1800 cm^{-1} [16]. The laser-induced fluorescent background was removed by the baseline correction algorithm by Cao *et al.* [17]. Subtraction of the pre-recorded contaminant spectrum was performed using the variance minimization method presented by Loethen *et al.* [18]. These algorithms were implemented in-house in MATLAB® (v. R2010a, MathWorks Inc., Natick, MA, USA). The treated spectra were vector normalized.

2.5. Cementing a steel pipe in the PZT element

A thin steel pipe (medical injection needle), with outer diameter 0.8 mm, was used as substitute for the actual RS probe when examining the optimal amount of rubber latex. The steel pipe were cemented in the hollow centre of the PZT element by filling the tube completely, 100%, or only half-full, 50%, with rubber latex (WackerElastisil RT622, WackerChemie GmbH, Munich, Germany) (figure 1). The gain and phase of the PZT-element response was monitored using a network analyser (Agilent E5100 A 10 kHz – 300 kHz Network Analyzer, Santa Clara, California, USA). The peak frequency shift and Q factor of the resonance peak at 114 kHz was investigated. The resonance peak's quality factor is described by the Q factor, equation (1) [19], where f_r and f_l are the frequencies at which the gain is -3 dB of the peak gain

$$Q = \frac{\sqrt{f_r \times f_l}}{f_r - f_l}. \tag{1}$$

The peak frequency and Q factor averages and standard deviations were determined.

2.6. Rise of temperature due to laser illumination

The temperature of the RS probe tip, the RS steel casing, and a PZT element mounted around the RS probe, was measured with an infrared camera system (ThermaCAM™ Researcher, FLIR Systems AB, Stockholm, Sweden) during RS measurements. The laser power was set from 20 mW to 270 mW, and repeated for 10-s and 20-s measurement times. A thin layer of Teflon tape was wrapped around the steel probe to increase the emissivity. A thick layer of Teflon tape was used to attach the PZT element around the RS probe. Both the recorded heating and cooling data were fitted to the model described by equation (2), using the Curve Fitting Toolbox v.2.2 in MATLAB®.

$$T = a \cdot e^{-t/\tau} + b \tag{2}$$

where T (°C) is the temperature after the time t (s) since the laser was switched on or off. The parameter τ is the thermal time constant and represents the time for the temperature to reach 1-1/e, *i.e.* 63%, of its initial value. The parameter b was set to room temperature, 30 °C, when modelling the cooling curve for powers of 240 mW and higher. For these powers, a higher measurement range in the IR camera was used, which did not record temperature values below 30 °C, and it was physically improbable that the probe would ever get cooler than its surroundings.

2.7. Impact of ambient light on RS

Enclosed inside a PZT element, the RS probe would be shielded from surrounding light when the combined probe is pressed against the measurement sample. A prototype light protective shield was mounted as a sleeve on the outside of the RS probe (figure 2). The sleeve had inner diameter 3 mm and outer diameter 6 mm. Aluminium disks with outer diameters 25 mm and 35 mm were attached to the sleeve to increase the shielding size. Three different bright environments were set up: direct incandescent light (252 lux), indirect incandescent light (15 lux), and indirect fluorescent light (82 lux). The direct light was provided by a 60 W incandescent light bulb situated approximately 80 cm away from the RS tip and sample. The indirect incandescent light was set up by directing the light to the white inner ceiling. The indirect fluorescent light was provided by two 28W/830 Lumilux Warm White fluorescent light tubes directed to the white inner ceiling. The illuminance for each light setting was measured at the sample using a Digital Light Meter (DVM1300 – LUXMETER, Velleman® Inc., Gavare, Belgium).

The light shields were evaluated in measurements on porcine muscle tissue. RS was performed in all three light settings with laser powers between 100 and 270 mW at both 5-s and 10-s integration times. Spectra were also collected without laser to acquire the contaminant spectra due to the surrounding light, and in dark at all settings to obtain dark spectra for comparison. Five replicate spectra were collected and mean spectra were calculated. These spectra were baseline corrected; the contaminant spectra were removed and then normalized. Raw and treated spectra were evaluated and compared to dark spectra by visual inspection.

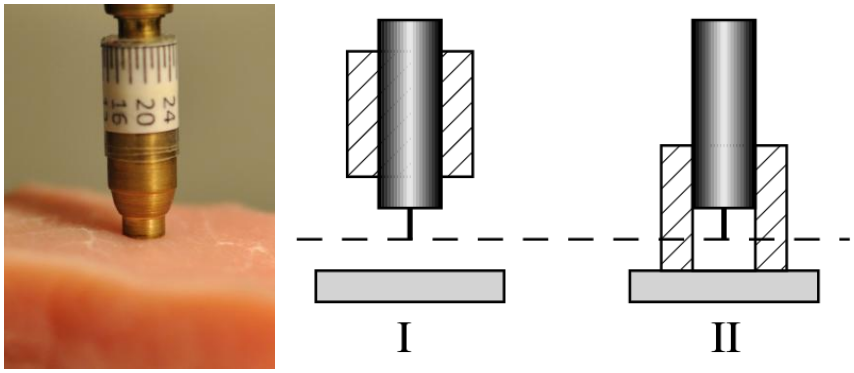

Figure 2. (Left) Photograph of the 6-mm prototype light protective shield in use. (Right) Raman probe with the shield retracted (I) and in use (II). The tip-to-sample distance is kept constant (dashed line). Aluminium disks with outer diameters of 25 or 35 mm are not shown in the figure.

3. Results

3.1. Cementing a steel pipe in the PZT element

The mean ± SD peak frequency for an empty PZT element was 114 149 Hz ± 54 Hz (n = 9). It was shifted the least when the 0.8-mm diameter steel pipe was cemented into the PZT element using 50% rubber latex, 114 056 Hz ± 58 Hz (n = 4) compared to 113 853 Hz ± 65 Hz (n = 5) for 100% rubber latex. Similar results were found for the Q factor. The Q factor for an empty PZT element was 133.1 ± 10.5 (n = 9). It was 99.2 ± 9.2 (n = 4) for 50% and 81.0 ± 4.1 (n = 5) for 100% rubber latex.

3.2. Rise of temperature due to laser illumination

The IR camera images showed that the tip of the RS probe was heated more than any other part when the laser was active (figures 3 and 4(a)). The surrounding PZT element was heated less than 2 °C at the highest laser power setting, 270 mW, and longest integration time, 20 s, and the heating occurred closest to the RS probe tip (figure 4(b)).

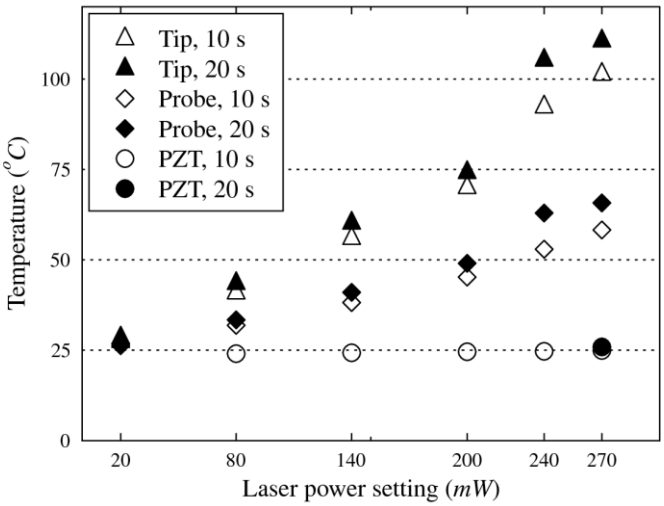

Figure 3. Maximal temperatures at the hottest sites during RS measurements.

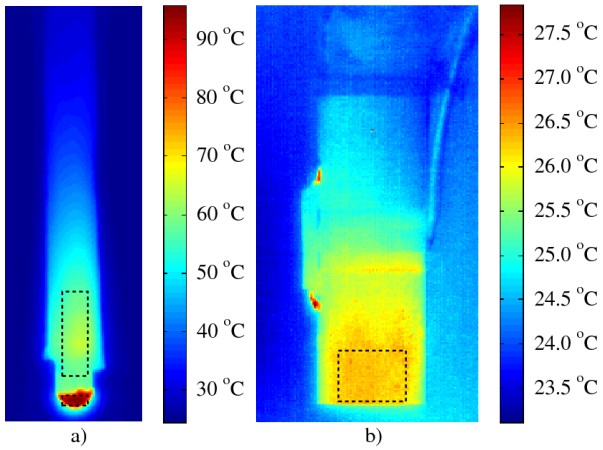

Figure 4. Temperature image of (a) the RS probe after 10 s at 240 mW and (b) the PZT element after 20 s at 270 mW. Average temperatures were calculated within the dashed rectangles.

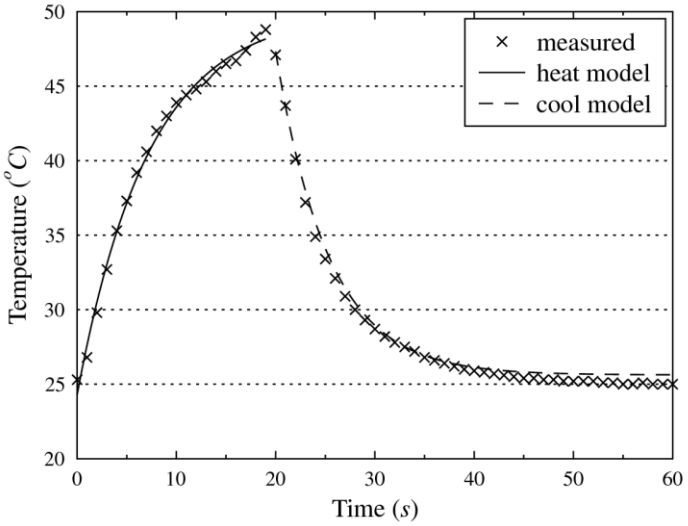

Figure 5. Representative curve for heating and cooling at the steel probe end. Measured temperature (x) at setting 200 mW 20 s, during heating (-) (τ_h = 7.2 s) and cooling (- -) (τ_c = 5.3 s) modeled by equation 1.

The RS steel probe was quickly heated and rapidly cooled (figure 5). The average heating thermal time constant, τ_h, was 6.8 s ± 1.6 s (mean ± SD) and the cooling thermal time constant, τ_c, was 4.2 s ± 1.0 s. The temperature of the steel probe dropped to 30 °C or below for all settings after 8 s, and to 27 °C or below after 13 s.

3.3. Impact of ambient light on RS

The "sleeve" shield with 6-mm outer diameter failed to prevent the detector from saturation at 10 s integration time for all laser powers but succeeded at 5 s. The additional 25-mm and 35-mm shields both prevented saturation in direct light at both 5 and 10-s integration times. Still, the RS spectra contained too much noise to allow a viable Raman spectrum to be extracted (table 1). Dimming the light by using indirect light, either incandescent and fluorescent, lowered the intensity of the contaminant spectra markedly even without any 25 or 35-mm shield (figures 6(b) and (e)). This made it possible to process the collected spectra and extract viable Raman spectra (table 1).

Table 1. Outcome from the visual inspection of the RS spectra for 5 and 10-s integration time settings when evaluating three light protective shields (6, 25, 35-mm) and three illumination settings (252, 15, 82 lux). The results are reported as 'Success after proc.' if the spectra were successfully treated by the algorithms; 'Saturated detector' if no spectrum could be extracted, 'Too high bkg' if considerable background artefacts remained after treatment; or 'Bkg peaks remaining' if sharp peaks from the background remained after treatment.

		Results (10 s)			Results (5 s)		
Illumination	Laser power	6-mm shield	25-mm shield	35-mm shield	6-mm shield	25-mm shield	35-mm shield
Incandescent (252 lux)	270 mW	Saturated detector	Too high bkg	Too high bkg	Too high bkg	Too high bkg	Too high bkg

Incandescent (252 lux)	200 mW	Saturated detector	Too high bkg	Too high bkg	Too high bkg	Too high bkg	Too high bkg
Incandescent (252 lux)	100 mW	Saturated detector	Too high bkg	Too high bkg	Too high bkg	Too high bkg	Too high bkg
Incandescent (15 lux)	270 mw	Success after proc.	Success after proc.	Success after proc.	Success after proc.	Success after proc.	Success after proc.
Incandescent (15 lux)	200 mW	Success after proc.	Success after proc.	Success after proc.	Success after proc.	Success after proc.	Success after proc.
Incandescent (15 lux)	100 mW	Too high bkg	Success after proc.	Success after proc.	Too high bkg	Success after proc.	Success after proc.
Fluorescent (82 lux)	270 mW	Bkg peaks remaining	Bkg peaks remaining	Bkg peaks remaining	Success after proc.	Success after proc.	Success after proc.
Fluorescent (82 lux)	200 mW	Success after proc.	Success after proc.	Success after proc.	Success after proc.	Success after proc.	Success after proc.
Fluorescent (82 lux)	100 mW	Success after proc.	Success after proc.	Success after proc.	Success after proc.	Success after proc.	Success after proc.

The 25-mm shield decreased the intensity of the raw spectra to 25% compared to the unshielded spectra obtained in indirect incandescent light (figure 6(c)), and the 35-mm shield decreased it to 15% (figure 6(d)).

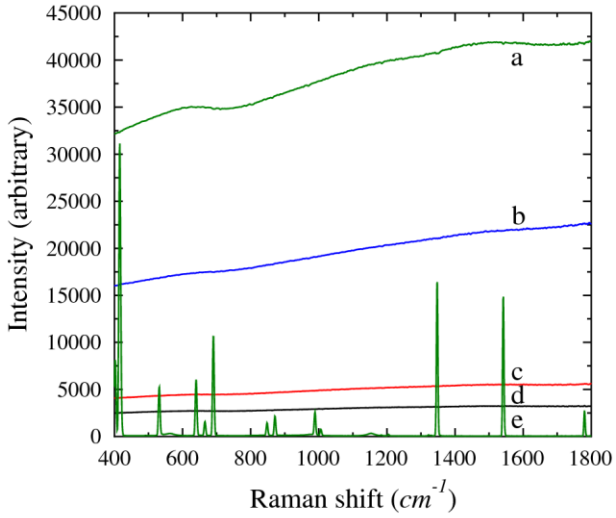

Figure 6. Relative intensities of raw contaminant spectra obtained in different light settings using different light shieldings. (a) 35-mm shield, 252 lux incandescent light; (b) no shield, 15 lux incandescent light; (c) 25-mm shield, 15 lux incandescent light; (d) 35-mm shield, 15 lux incandescent light; and (e) no shield, 82 lux fluorescent light. 0 mW 10 s for all spectra.

Raman spectra were successfully extracted from the contaminated spectra by the algorithms when using the 25 or 35-mm shields and indirect light. The 25-mm shield reduced the intensity of the raw contaminant spectra (figure 7(c)) compared with the unshielded spectra (figure 6(b) and 7(a)). This allowed performing RS using settings that are assumed clinically acceptable (200 mW, 10 s) in a dimmed but relatively bright

environment (15 lux), yielding an acceptable raw spectrum (figure 7(b)). By subtracting pre-recorded background spectra and performing baseline correction, the normalized RS spectra obtained in light becomes very similar to baseline-corrected and normalized RS spectra recorded in the dark (figures 7(d) and (e)). The results for 5-s integration times were similar.

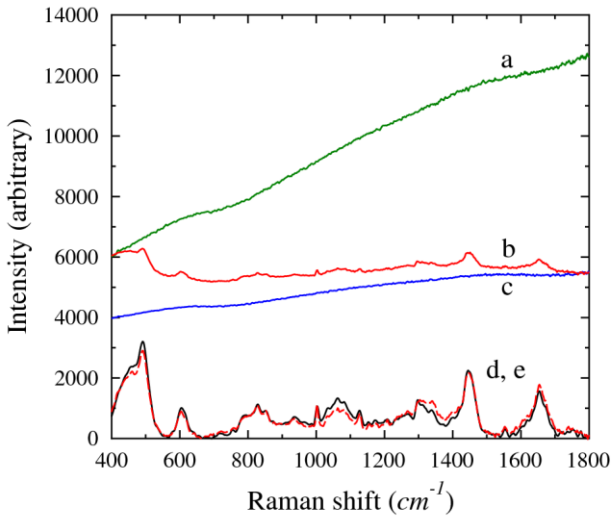

Figure 7. Raman spectra of porcine muscle for 10 s and 15 lux incandescent light. (a) Raw background spectrum using no shield, reduced by 10000 counts; (b) raw spectrum, 200 mW, 10 s, 25–mm shield; (c) raw background spectrum using 25-mm shield; (d) treated spectrum, 200 mW, 10 s, 25-mm shield, normalized and arbitrary scaled; (e) and dark spectrum (0 lux), 200 mW, 10 s, normalized and arbitrary scaled.

4. Discussion

This study investigated several topics important for the design of a combination probe for tissue characterization using RS and TRM. More specifically they were:

- the effect of attaching a 0.8-mm diameter fibre-optic RS probe into a tube-shaped TRM sensor,
- the magnitude and time scale of the laser-induced heating of the RS probe tip,
- the feasibility to perform fibre-optic RS in bright environments with the following factors in mind:
    - the RS laser power,
    - the RS integration time,
    - the light shield size,
    - the type of the surrounding light,
    - a set of background-reducing algorithms.

Throughout the study, laser power and integration times were chosen to reflect the actual settings that might be used in a clinical situation. Moreover, temperature intervals and surrounding light settings were chosen to mimic real life situations.

4.1. Cementing a steel pipe in the PZT element

The uses of piezoelectric ceramics as tactile sensors have previously not incorporated a rigid piston inside a cylindrical resonance sensor element. Earlier sensor elements have been flat and rectangular [20, 21] or cylindrical with attachments on the outside of the element [15, 22, 23].

Thin steel pipes, in the form of medical injection needles, were used to model the RS probe, because the final 10 cm of the RS probe is embedded in a stainless steel tube. Development of an earlier TRM instrument has shown that rubber latex is appropriate for mounting PZT elements in the sensor housing [22]. The resonance frequency and the Q factor changed when a steel pipe was attached inside the cylindrical PZT element. The two properties were affected correspondingly by the size of the steel pipe and the amount of rubber cement. The largest effect was noted when using the steel pipe of greater diameter, as shown in a previous study [24]. This was probably because it made the layer of compliant rubber cement thinner, and therefore stiffer, between the inner wall and the rigid steel pipe. The steel pipe appeared to act as reinforcement to the cement, as noticed when the steel pipes were removed, leaving the cement in the PZT element. In this study, the amount of rubber latex filling was investigated further for a 0.8-mm diameter steel pipe. A larger amount of rubber latex changed the resonance frequency and Q factor more when the larger steel pipe was attached. The amount of rubber latex was less influential when attaching the smaller steel pipe. This study showed that when an RS probe is integrated into a cylindrical PZT element, the free space between the RS probe and the inside of the PZT element should not be completely filled with rubber cement if small changes in the base frequency and signal quality are to be measured.

4.2. Rise of temperature due to laser illumination

The RS tip might cause heat-induced damage to biological tissue if it becomes too hot. The temperature for thermal damage is different for almost every tissue type and macromolecule [25]. However, DNA and RNA typically withstand temperatures up to 85 °C without damage according to Bischof *et al.* [26]. This agrees with data for DNA and RNA presented by Despa *et al.* for a 10-s mid-dermis exposure at 80 °C [25]. The temperature of the RS tip remained lower than 75 °C if higher laser powers than 200 mW were avoided (figure 3). Although tissue damages at temperatures in the range of 60-70 °C has been reported [27-28], no adverse effects or tissue damage was noticed during RS using this experimental setup, other than a slight dehydration of the tissue at the measurement spot. Furthermore, the RS tip is not intended to touch the tissue directly. Its optimum distance is approximately 0.4 mm from the tissue [10]. In the combined probe, the RS tip will be encased by the TRM tip, preventing direct contact by the RS tip with the tissue. The temperature of the RS probe tip quickly rose and sank when the laser shutter was opened and closed (figure 5). In a combined instrument, the RS modality is intended to be used sparingly. The combination allows for a fast probing using the TRM alone, and RS is only used when the possibility of a tumour is found. This means that there is plenty of opportunity to disperse the induced heat. The temperature of the steel probe dropped to 30 °C or below for all settings after 8 s, and to 27 °C or below after 13 s. The IR camera system visualized the temperature along the length of the RS probe. It became evident that the heat production was located to the tip of the RS probe. This was even more evident in the IR image of the steel probe without the PZT element (figure 4(a)). The heat spreads along the RS steel probe and transfers to the TRM sensor. Due to the larger specific heat capacity of the PZT element, the temperature rise is smaller and will not exceed 5 °C (figures 3 and 4(b)). Assuming a specific heat capacity of 0.35 J/(g K) [29], one can estimate an approximate temperature of the PZT element. The actual laser output power was approximately 47% of the set laser power. The lost power is probably converted into heat at the end filter and end lens. If 100 mW is converted during 10 s, then the 1.6-g PZT element would rise maximally 1.8 °C due to the transfer of 1.0 J energy as heat.

4.3. Impact of ambient light on RS

Besides all other restrictions that have to be considered, it should also be possible to use a combined probe in a bright environment. The usefulness of a clinical instrument would otherwise be limited.

The surrounding light has to be removed from the signal. To succeed with this, the quality and intensity of the surrounding light is very important. A shield helps when the light is not too bright to begin with. A combination of algorithms and a pre-recorded contaminant spectrum of the surrounding light are necessary for extracting a good Raman spectrum.

The relatively low probability that a photon will be scattered by the Raman principle has at least two consequences: the ratio between Raman scattered light and incident light is low, and the RS detectors are very sensitive to light. The former is remedied by using intense monochromatic light. The elastically scattered monochromatic light is prevented from reaching the detector by an edge filter, and elastically scattered monochromatic light would not really impose a problem *per se*. Stray light from surrounding bright environments can quickly drench the weak Raman signal in the RS spectrum. Biological tissue is translucent to 785 nm – 1100 nm light [30, 31]. The 6-mm diameter light-protective shield performed well when obtaining Raman spectra from the solid silicone sample in a preliminary test but yielded almost no effect with porcine tissue samples. Therefore, more than a simple 6-mm shield is needed. Scaffidi *et al.* recently showed a proof-of-concept when they applied subtraction of situation-specific background spectra [32]. Also, it is not necessary to illuminate the biological sample with the brightest of lights during the RS measurement. The laser power was limited to 270 mW to avoid overheating the fibre-optic probe. Measurement times of 5-10 s were assumed appropriate to mimic a future clinical situation. Different light situations were set up by directing the incandescent light either directly towards the biological sample or towards the inner ceiling. The use of fluorescent light was also investigated.

When not using light directed directly at the tissue sample, acceptable RS spectra were obtained using a laser power of 200 mW for 10 s or less (table 1 and figure 7). The CCD detector became fully saturated when incandescent light fell directly onto the sample, unless protected by the 25-mm light shield. The effect of the light shield could be estimated while using indirect incandescent light, which yielded approximately 22 000 CCD counts around 1600 cm^{-1} (figure 6(b)). The 25-mm light shield lowered the intensity to 5500 CCD counts and the 35-mm light shield yielded 3200 CCD counts (figures 6(c) and (d)), which corresponds to 25% and 15%, respectively. This shows that the larger light shield substantially lowers the amount of surrounding light that reaches the detector. It also suggests that the shield diameter could be made smaller than 25 mm if decreasing the intensity of the surrounding light would avoid detector saturation. The pre-recorded spectra caused by the surrounding light were successfully subtracted from the RS spectra by the algorithm suggested by Loethen *et al.* when the light was not direct (figure 7). The bright, direct light caused high amplitude, random noise that was not sufficiently blocked by the 35-mm light shield, even though it prevented the detector from being saturated. Decreasing the intensity of the incandescent light, and shielding the probe with a 25-mm light shield, allowed the combined algorithms suggested by Cao *et al.* and Loethen *et al* to subtract all traces of contamination from the mixed spectra to such an extent that it became virtually identical to a spectra obtained in complete darkness (figures 7(d) and (e)).

At 200-mW laser power and 10-s integration time, which allowed for RS with surrounding light, the temperature of the RS probe tip was increased to 70°C, but the temperature rise of the PZT element was barely noticeable. This small change in temperature was lower than the temperature variations for which the Venustron system's reliability has been previously investigated [24]. The theoretical maximum temperature rise due to the dissipated power and the thermal heat capacity of the PZT element was also moderate (< 2 °C). The RS laser power and integration time is therefore not restricted by adding a TRM device. However, the laser power has to be restricted to avoid the RS probe tip from burning the tissue as the tip's temperature increased to over 100 °C when set to 270-mW laser output. The temperature rise is not high enough to destroy the TRM sensor by passing the Curie temperature or other important piezoelectric parameters [33]. The heating of the RS probe might restrict the choice of material used to

manufacture the combined probe near the RS probe tip. Furthermore, the RS probe tip would never come in direct contact with the investigated tissue as it is to be encased inside a TRM sensor.

Jalkanen [34] has shown that it is feasible to develop a hand-held instrument for measuring the prostate tissue stiffness using the tactile resonance technique. Together with the findings in this study, this would be the basis to say that a hand-held device that combines RS and TRM would be possible to build.

5. Conclusion

The results of this study showed that a combination of the TRM and fibre-optic RS is feasible. It also reveals important restrictions and limitations that have to be considered in the design of a working prototype.

It can be concluded that the impact of cementing an RS probe, here modelled as a thin steel pipe, is minimized when a small amount of rubber cement is used. The heat induced by the RS laser causes an acceptable small temperature rise in the PZT element, and the heat is quickly dissipated. The heat induced in the RS tip by the laser may possibly be kept below a damage-inducing level while using RS settings appropriate for acquiring usable RS spectra in bright environments. In a combined instrument it is recommended to wait until cooling is attained. A final conclusion was that it was possible to perform RS in relatively bright environments by carefully designing the surrounding light and using light shields of appropriate size. The study successfully evaluated a set of background-reducing algorithms that removed the remaining effects of the bright environment. Considering these results in the design of the probe, we suggest that it may be possible to integrate RS and TRM in a combined instrument for tissue characterization.

Acknowledgement

This work was supported by grants from the Objective 2 Norra Norrland-EU Structural Fund and the Kempe Foundation.

References

[1] Lorincz A, Haddad D, Naik R, Naik V, Fung A, Cao A, Manda P, Pandya A, Auner G, Rabah R, Langenburg S E, and D. Klein M D 2004 Raman Spectroscopy for Neoplastic Tissue Differentiation: A Pilot Study *J Pediatr Surg* **39** 953-6

[2] Stone N, Kendall C, Shepherd N, Crow P, and Barr H 2002 Near-infrared Raman spectroscopy for the classification of epithelial pre-cancers and cancers *J. Raman Spectrosc.* **33** 564-73

[3] Takei M, Shiraiwa H, Omata S, Motooka N, Mitamura K, Horie T, Ookubo T, Sawada S 2004 A new tactile skin sensor for measuring skin hardness in patients with systemic sclerosis and autoimmune Raynaud's phenomenon *J Int Med Res.* **32** 222-31.

[4] Miyaji K, Furuse A, Nakajima J, Kohno T, Ohtsuka T, Yagyu K, Oka T, Omata S 1997 The stiffness of lymph nodes containing lung carcinoma metastases *Cancer* **80** 1920-5

[5] Kusaka K, Harihara Y, Torzilli G, Kubota K, Takayama T, Makuuchi M, Mori M, Omata S 2000 Objective evaluation of liver consistency to estimate hepatic fibrosis and functional reserve for hepatectomy *J Am Coll Surgeons* **191** 47-53

[6] Crow P, Barrass B, Kendall C, Hart-Prieto M, Wright M, Persad R, and Stone N 2005 The use of Raman spectroscopy to differentiate between different prostatic adenocarcinoma cell lines *Br. J. Cancer* **92** 2166-70 (doi: 10.1038/sj.bjc.6602638)

[7] Jalkanen V, Andersson B M, Bergh A, Ljungberg B, and Lindahl O A 2007 Spatial variations in prostate tissue histology as measured by a tactile resonance sensor *Physiol. Meas.* **28** 1267-81 (doi:10.1088/0967-3334/28/10/011)

[8] Jalkanen V, Andersson B M, Bergh A, Ljungberg B, and Lindahl O A 2006 Prostate tissue stiffness as measured with a resonance sensor system: a study on silicone and human prostate tissue in vitro *Med. Bio. Eng. Comput.* **44** 593-603 (doi:10.1007/s11517-006-0069-6)

[9] Candefjord S, Nyberg M, Jalkanen V, Ramser K, and Lindahl O A 2010 Combining fibre optic Raman spectroscopy and tactile resonance measurement for tissue characterization *Meas. Sci. Technol.* **21** 125801-8 (doi:10.1088/0957-0233/21/12/125801)

[10] Komachi Y, Sato H, Aizawa K, and Tashiro H 2005 Micro-optical fiber probe for use in an intravascular Raman endoscope *Appl. Opt.* **44** 4722-32 (doi:10.1364/AO.44.004722)

[11] Ferraro J R, Nakamoto K, and Brown C W 2003 *Introductory Raman Spectroscopy*. San Diego: Academic Press

[12] Komachi Y, Katagiri T, Sato H, and Tashiro H 2009 Improvement and analysis of a micro Raman probe *Appl. Opt.* **48** 1683-96 (doi:10.1364/AO.48.001683)

[13] Cady W G 1946 *Piezoelectricity, an Introduction to the Theory and Applications of Electromechanical Phenomena in Crystals.* London: McGraw-Hill Book Company, Inc.

[14] Motz J T, Hunter M, Galindo L H, Gardecki J A, Kramer J R, Dasari R R, and Feld M S 2004 Optical fiber probe for Biomedical Raman spectroscopy *Appl. Opt.* **43** 542-54 (doi:10.1364/AO.43.000542)

[15] Eklund A, Bergh A, and Lindahl O A 1999 A catheter tactile sensor for measuring hardness of soft tissue: measurement in a silicone model and in an *in vitro* human prostate model *Med. Biol. Eng. Comput.* **37** 618-24

[16] Beattie JR, Bell SE J, Borggaard C, Fearon A M, Moss B W 2007 Classification of adipose tissue species using Raman spectroscopy *Lipids* **42** 679-85 (doi:10.1007/s11745-007-3059-z)

[17] Cao A *et al.* 2007 A robust method for automated background subtraction of tissue fluorescence *J. Raman Spectrosc.* **38** 1199-1205 (doi:10.1002/jrs.1753)

[18] Loethen Y L, Zhang D, Favors R N, Basiaga S B G, and Ben-Amotz D 2004 Second-derivative variance minimization method for automated spectral subtraction *Appl. Spectrosc.* **58** 272-8 (http://www.opticsinfobase.org/abstract.cfm?URI=as-58-3-272)

[19] Agilent, (2001) Agilent E5100A/B Network Analyzer Function Reference. Agilent Technologies Japan, Ltd. Component Test PGU-Kobe 1-3-2, Murotani, Nishi-ku, Kobe-shi, Hyogo, 651-2241 Japan

[20] Omata S and Terunuma Y 1992 New tactile sensor like the human hand and its applications *Sens. Actuators A* **35** 9–15 (doi:10.1016/0924-4247(92)87002-X)

[21] Hallberg P, Linden C, Lindahl O A, Backlund T, and Eklund A 2004 Applanation resonance tonometry for intraocular pressure in humans. *Physiol. Meas.* **25**, 1053-65

[22] Hallberg P, Linden C, Backlund T, and Eklund A 2006 Symmetric sensor for applanation resonance tomometry of the eye *Med. Biol. Eng. Comput.* **44** 54-60 (doi:10.1007/s11517-005-0005-1)

[23] Murayama Y, Constantinou C E, and Omata S 2005 Development of tactile mapping system for the stiffness characterization of tissue slice using novel tactile sensing technology *Sens. Actuators A* **120** 543-9 (doi:10.1016/j.sna.2004.12.027)

[24] Nyberg M, Ramser K, and Lindahl O A 2009 Cancer detection probe combining Raman and resonance sensor technology – Experimental study on temperature dependence and effects of molding *IFMBE Proceedings* **25** 331-4 (doi:10.1007/978-3-642-03885-3_92)

[25] Despa F, Orgill D P, Neuwalder J, and Lee R C 2005 The relative thermal stability of tissue macromolecules and cellular structure in burn injury *Burns* **31** 568-77 (doi:10.1016/j.burns.2005.01.015)

[26] Bischof J C, He X 2005 Thermal stability of proteins *Ann. NY. Acad. Sci.* **1066** 12-33 (doi:10.1196/annals.1363.003)

[27] Rem A I, Oosterhuis J A, Journée-de Korver H G, van den Berg T J T P, Keunen J E E 2001 Temperature Dependence of Thermal Damage to the Sclera: Exploring the Heat Tolerance of the Sclera for Transscleral Thermotherapy *Exp. Eye Res.* **72** 153–62 (doi:10.1006/exer.2000.0939)

[28] Thomsen S, Pearce J A 1989 Changes in birefringence as markers of thermal damages in tissue *IEEE T. Bio-med. Eng.* **36** 1174–9 (doi:10.1109/10.42111)

[29] Yarlagadda S, Chan M H W, Lee H, Lesieutre G A, and Jensen D W 1995 Low temperature thermal conductivity, heat capacity and heat generation of PZT *J. Intell. Mat. Sys. Struct.* **6** 757-64

[30] Welch A J, Torres J H, Cheong W F 1989 Laser physics and laser-tissue interaction *Tex. Heart Inst. J.* **16** 141-9

[31] Krafft C, Steiner G, Beleiters C, and Salzer R 2009 Disease recognition by infrared and Raman spectroscopy *J. Biophoton.* **2** 13–28 (doi:10.1002/jbio.200810024)

[32] Scaffidi J P, Gregas M K, Lauly B, Carter J C, Angel S M, and Vo-Dinh T 2010 Trace Molecular detection via surface-enhanced Raman scattering and surface-enhanced resonance Raman scattering at a distance of 15 meters *Appl. Spectrosc.* **64** 485-92 (doi:10.1366/000370210791211763)

[33] Miclea C, Tanasoiu C, Amarande L, Miclea C F, Plavitu C, Cioangher M, Trupina L, Miclea C T, and David C 2007 Effect of temperature on the main piezoelectric parameters of a soft PZT Ceramic *Romanian Journal of Information Science and Technology* **10** 243-50

[34] Jalkanen V 2010 Hand-held resonance sensor for tissue stiffness measurements – a theoretical and experimental analysis *Meas. Sci. Technol.* **21** 055801-8 (doi:10.1088/0957-0233/21/5/055801)